Investigation of the temperature and DOD effect on the performance-degradation behavior of lithium–sulfur pouch cells during calendar aging

Capkova, Dominika; Knap, Vaclav; Strakova Fedorkovaa, Andrea; Stroe, Daniel-Ioan

Published in:
Applied Energy

DOI (link to publication from Publisher):
10.1016/j.apenergy.2022.120543

Publication date:
2023

Document Version
Early version, also known as pre-print

Highlights

Investigation of the Temperature and DOD Effect on the Performance-Degradation Behavior of Lithium-Sulfur Pouch Cells During Calendar Aging

Dominika Capkova,Vaclav Knap,Andrea Strakova Fedorkova,Daniel-Ioan Stroe

- Calendar aging tests of 3.4 Ah lithium-sulfur pouch cells have been investigated.
- Capacity loss is affected by temperature and depth-of-discharge during storage.
- Differential voltage analysis was used to study the calendar aging of Li-S batteries.
- Storage at low depth-of-discharge causes accelerated battery degradation.
- The increase in resistance was observed during storage in the discharged state.

Investigation of the Temperature and DOD Effect on the Performance-Degradation Behavior of Lithium-Sulfur Pouch Cells During Calendar Aging

Dominika Capkova[a,*], Vaclav Knap[b], Andrea Strakova Fedorkova[a] and Daniel-Ioan Stroe[c]

[a]Department of Physical Chemistry, Pavol Jozef Šafárik University in Košice, 041 54 Košice, Slovak Republic
[b]Faculty of Electrical Engineering, Czech Technical University in Prague, 166 27 Prague, Czech Republic
[c]Department of Energy, Aalborg University, 9220 Aalborg East, Denmark

ARTICLE INFO

Keywords:
Li-S pouch cell
Battery degradation
Calendar aging
Differential voltage analysis
Self-discharge

ABSTRACT

High-energy density sulfur cathodes are one of the most promising possibilities to replace currently used intercalation cathodes in lithium-ion batteries in future applications. However, lithium-sulfur batteries are still the subject of research due to unsatisfactory capacity retention and cycle performance. The cause of insufficient properties is the shuttle effect of higher polysulfides which are formed in a high voltage plateau. In an effort to optimize storage conditions of lithium-sulfur (Li-S) batteries, long-term calendar aging tests at various temperatures and depth-of-discharge were performed on pre-commercial 3.4 Ah Li-S pouch cells. The decrease in performance over two years of calendar aging in five stationary conditions was analyzed using non-destructive electrochemical tests. The negative effect on Li-S cell performance was more pronounced for temperature than for depth-of-discharge. The analyses of self-discharge and shuttle current were performed and as expected, the highest values were measured in a fully charged state where higher polysulfides are present. Furthermore, internal resistance was analyzed where an increase of resistance was observed for a discharged state due to the formation of a passivation layer from discharge products (Li_2S_2, Li_2S). To maximize the life of the Li-S battery, storage at high temperatures and in a fully charged state should be avoided.

1. Introduction

To satisfy the demand for efficient energy storage utilized in portable electronic devices, electric vehicles, and aerospace devices, the development of high-energy density battery systems is an essential mission for researchers. The rechargeable lithium-ion (Li-ion) batteries play a major role in the energy storage industry, although the practical energy density of current Li-ion batteries is not satisfactory for the future energy market [1, 2, 3, 4]. Research in next-generation battery systems, including lithium-sulfur (Li-S) batteries, is critical to the development of efficient, lighter, and lower-cost high-energy density batteries [5, 6, 7, 8]. The main advantage of Li-S batteries is the high theoretical capacity of sulfur (1675 Ah kg^{-1}), and the high theoretical gravimetric energy density, which is above 2600 Wh kg^{-1} despite lower operational voltage against lithium (∼2.1 V) [9, 10, 11, 12].

The successful commercialization of Li-S batteries is impeded mainly by their limited cycle performance, short lifetime, high self-discharge rate, and low efficiency [13, 14, 15]. These problems are related to several major issues, the main drawback of Li-S batteries is a dissolution of intermediates - polysulfides with long-chain (Li_2S_8, Li_2S_6, Li_2S_4) - in a liquid organic electrolyte and their migration between the electrodes, this process is known as the shuttle effect [16, 17, 18]. Li-S batteries suffer from poor electrical conductive properties of sulfur and solid discharge products (Li_2S_2, Li_2S). Moreover, they are exposed to a high mechanical stress caused by volumetric expansion during cycling up to 80 % [19, 20]. To solve these issues and prolong battery life, many improvements have been considered e.g., an encapsulation of sulfur into carbon materials with high surface area, e.g. amorphous carbons [21, 22, 23], graphene [24, 25], graphene oxides, or reduced graphene oxides [26, 27] and metal-organic frameworks (MOFs) [11, 28]. A stable long cycle life of batteries may be realized by electrolyte modification [29, 30, 31]. Battery lifespan may be limited by an uncontrollable growth of lithium dendrites [32]. Strategies for lithium anode protection include construction of protective layers [33, 34], lithium slats [35] and additives in the electrolyte [36, 37]. Application of mentioned

*Corresponding author
E-mail: dominika.capkova@upjs.sk (D. Capkova)
ORCID(s): 0000-0002-3614-5629 (D. Capkova); 0000-0003-0108-1714 (V. Knap); 0000-0002-2938-8921 (D. Stroe)

materials and methods to improve battery properties are often supported by theoretical work, and vice versa [38, 39, 40]. However, most of the research has been conducted on small laboratory set up, e.g. coin cells, and small pouch cells. The small-scale research provides the necessary fundamental information. However, the disadvantage is that some phenomena cannot be observed at easily measurable levels, as would be in the case of a larger cell (e.g. thermal response) [41].

In order to accelerate the commercialization of Li-S batteries, it is necessary to study the aging of batteries under realistic conditions that arise due to cycling and time. Due to this fact, battery degradation can be distinguished into cycling (during use) and calendar (on storage) [42]. The degradation of active materials, irreversible relocation of polysulfides, volume changes, concentration gradients, and lithium plating at the anode are results of cycling aging. In general, all kinetic processes are included in aging during cycling. Contrary, the calendar aging process is connected to the thermodynamic instability of materials as a result of side reactions. During storage, the battery is affected by the reaction of the interphase between the electrode and electrolyte, polysulfide diffusion, and self-discharge [42, 43, 44]. The state of charge and the temperature at which the battery is stored are fundamental factors influencing calendar aging as they determine the concentration gradient of species and rate of chemical reactions [45]. Calendar life can be monitored by loss of capacity, potential change, and increase of impedance [46, 47, 48]. However, calendar aging cannot be straightforwardly separated from cycling aging during battery operation.

Electrochemistry of degradation mechanism in Li-S batteries during cycling is well described for different electrode materials, lithium metal anode, or electrolytes [49, 50, 51]. The majority of aging studies focus on small-scale testing and one research presents cycling aging of 19 Ah Li-S pouch cell [52]. Less attention is paid to self-discharge and calendar aging, the publications mostly deal with short-term self-discharge studies [44, 53, 54], or cells stored at one condition [55]. The self-discharge behavior of Li-S batteries was studied using polymer electrolyte and liquid electrolyte on a small scale [56, 57] and on Li-S pouch cells for a short time period [58]. The self-discharge, discharge capacity, and efficiency are affected by the polysulfide shuttle process. The redox shuttle and its impact on the behavior of the Li-S battery were first quantitatively described by Mikhaylik and Akridge [18] through the combination of mathematical modeling and experiments. The highest shuttle current was observed close to the maximum value of state-of-charge where the long-chain polysulfides are formed. The measurement of shuttle current may be useful to predict the cycle life and degradation of Li-S cell [59, 60].

This paper deals with an in-depth analysis of long-term calendar aging of pre-commercial 3.4 Ah Li-S pouch cells. Groups of cells were held at storage conditions that comprised three temperature levels and discharge depths. The evaluation of total capacity, the capacity of high and low voltage plateau, and Coulombic efficiency are analyzed and discussed. Furthermore, incremental capacity analysis (ICA) and differential voltage analysis (DVA) are applied to deeply analyze differences in battery degradation. The influence of the shuttle effect during storage was quantified by measurement of shuttle current and self-discharge and their development with time. Moreover, the calendar aging of the Li-S batteries was investigated by analyzing the resistance behavior obtained from current pulses and electrochemical impedance spectroscopy (EIS). All these methods enabled to study degradation behavior and help to identify the predominant mechanisms of aging without destructive analysis. The most significant effect on the capacity drop of the Li-S battery is the storage in a high temperature and charged state, where higher polysulfides are involved in the shuttle effect. Li-S cells should be stored at depth-of-discharge higher than 30 % corresponding to the capacity of the high voltage plateau. High self-discharge rate (in the early stage up to 70 % and stabilized around 20 % after 27 months) and high shuttle current (up to 0.2 A) are observed during storage at low depth-of-discharge.

2. Non-destructive techniques for battery degradation diagnostics

2.1. Incremental Capacity Analysis and Differential Voltage Analysis

Incremental capacity analysis (ICA) has attracted tremendous attention of researchers as it can track and identify various material and electrochemical changes during charging [61, 62]. The ratio between the increment of capacity and the associated voltage (dQ/dV) generates the IC curve and the IC peaks with different intensities are formed [63]. Using the inverse ratio (dV/dQ) we obtain differential voltage analysis (DVA) [64]. The changes in the IC and DV curves may help to investigate the internal changes in batteries and aging mechanism degrading battery performance (e.g. loss of active material). However, these methods have not been widely applied to Li-S batteries and can not be directly transferred from Li-ion to Li-S. Thus, change in implementation and interpretation has to be considered.

Table 1
Specifications of the prototype Li-S pouch cell.

Parameter	Value
Nominal Capacity	3.4 Ah
Nominal Voltage	2.05 V
Maximum Voltage	2.45 V
Minimum Voltage	1.5 V
Nominal Charging Current	0.34 A (0.1 C)
Nominal Discharging Current	0.68 A (0.2 C)
Temperature Operation Range	+5 °C to +80 °C

2.2. Self-Discharge Measurement

The reversible loss of battery capacity after a period of storage is generally called self-discharge and always occurs when batteries are resting [65]. The concept of direct measurement of self-discharge is based on charging the cell to a target depth-of-discharge/depth-of-charge (DOD/DOC), resting the cell for a set period (open-circuit voltage (OCV) monitoring is possible), and discharging the cell to determine the capacity lost. However, the self-discharge rate depends on the time elapsed since recharging and will vary for different idle times [66]. The polysulfide shuttle effect induces strong self-discharge within several hours of storage and the capacity self-discharges around 30 % in a charged state of battery which corresponds with the capacity of high voltage plateau [11, 67, 68].

2.3. Measurement of Shuttle Current

Since the reaction mechanism and side reactions of Li-S batteries have not yet been fully described and understood, the measurement of the shuttle current may provide important insights into the ongoing process of polysulfide shuttle and predict the degradation of batteries. The measurement of shuttle current may be performed in a direct [59, 60] and continues way [69]. The direct shuttle current measurement method is based on constant voltage operation and monitoring of the current value until it reaches steady-state, which is considered that shuttle current. [59]. The calculation of shuttle current using the continuous method is based on the voltage-capacity relationship between two consecutive discharge cycles as presented by Maurer et al. [69]. A high concentration of the higher-order polysulfides causes an increase in shuttle current.

2.4. Electrochemical Impedance Spectroscopy

Electrochemical impedance spectroscopy (EIS) is a non-destructive technique established as a powerful tool for exploring transport properties of materials, electrochemical mechanisms, reaction kinetics, battery life performance, and investigation of the properties of porous electrodes. The current is measured at applied potential (galvanostatic mode) in the frequency domain. The results are interpreted in terms of linear systems theory and the data validity can be designated by Kramers-Kronig (K-K) transforms [70, 71]. The complex value of the impedance (Z) can be obtained from the ratio of voltage to current amplitude and phase lag of output and input. It is possible to separate impedance in a real part (Z') and imaginary part (Z"), these two parts can be displayed in complex plane plots (Nyquist plots) in order to visualize the impact of parameters [72]. The EIS analysis is widely used to investigate the electrochemical processes in Li-S batteries, to study their degradation mechanisms, the effect of temperature, electrochemical reactions during charging or discharging at different DOD/DOC, and estimation of state-of-health (SOH) [73, 74, 75, 76, 77]. An EIS spectrum typical for Li-S batteries is usually formed by two semicircles in high and middle-frequency regions and an oblique line in the low-frequency area [73]. The experimental EIS spectra can be fitted by an equivalent circuit through a numerical optimization of circuit parameters [78].

3. Methodology

The Li-S cells that are considered in this study are pre-commercial long-life pouch cells (OXIS Energy) with a rated capacity of 3.4 Ah and sandwich structure. A mixture of sulfur, carbon, and binder coated on the current collector represents the cathode. Metallic lithium is used as the anode and the separator is saturated by a sulfolane-based electrolyte. Specifications of investigated 3.4 Ah Li-S pouch cells are listed in Table 1.

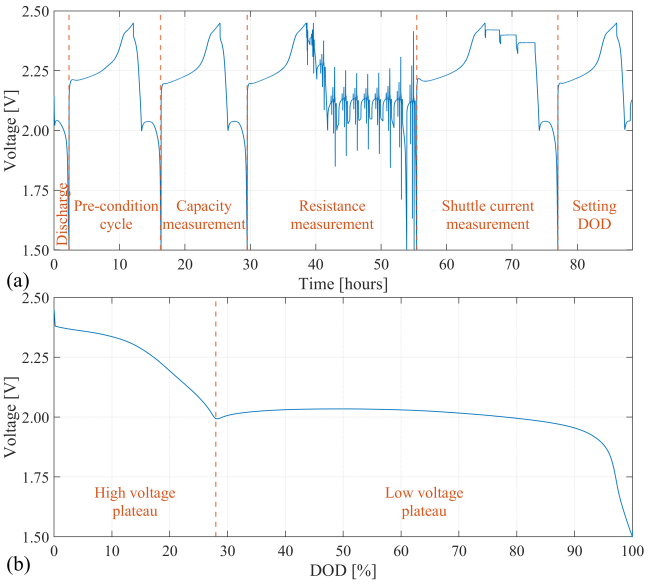

Fig. 1: (a) Illustration of the RPT procedure and (b) the discharge profile of the Li-S pouch cells.

The measurement methodology of calendar aging consisted of a reference performance test (RPT), which was performed periodically every month during storage. A detailed description of the applied RPT procedure is given in [79] and illustrated in Fig. 1, according to the following set up:

1. Discharging of the cell to obtain the remaining capacity after shelf storage;
2. To reset 'the cumulative history' of the cell a precondition cycle was performed;
3. The measurement of actual charge and discharge capacity;
4. A set of charging and discharging pulses were applied at various DOD/DOC levels to obtain the resistance of the cell;
5. For every even RPT measuring of the shuttle current or EIS;
6. Charging followed by discharging of the cell to target DOD level.

The cells were always charged by 0.34 A (0.1 C) and discharged by 0.68 A (0.2 C). The charging was limited by a cut-off limit of 2.45 V or 11 hours and the cut-off limit for discharging was 1.5 V. Each test case was performed on two Li-S cells to demonstrate the reproducibility of the experiment. To extend the battery characterization the shuttle current was measured on one cell and EIS on the other.

A Digatron BTS 600 battery tester was used for RPTs. The EIS measurements were performed at FuelCon Evaluator B Battery Test Station. During the RPTs and calendar aging, the cells were stored in a controlled temperature environment in thermal chambers. The reference temperature for the RPTs was 30 °C. Before the beginning of the test, the cells were allowed to thermally stabilize for two hours. At the end of the RPTs, the cells' DOD was set to specific values. In this study, the values 0, 50, and 90 % were used. Moreover, three levels of storage temperature were considered, i.e. 7.5, 30, and 50 °C. Overall, there were five calendar cases applied on ten Li-S pouch cells. The overview of the specific calendar test conditions is presented in Table 2.

The detailed interpretation of capacity changes can be found in Section 4. The ICA/DVA analyses presented in this paper are established based on a method presented by Knap and coauthors [80] and elaborated in Section 5. The IC curve was obtained from the voltage evolution curve under a constant-current charging regime. Before further ICA analysis, the original data were carefully de-noised via Savitzky-Golay filtering (settings: 3rd order and 21 sample window for voltage, 1st order and 101 sample window for capacity) and moving average (with windows of 3 samples and 2 samples for voltage and capacity, respectively). Subsequently, derivative calculation of charging capacity to battery voltage was performed for IC curve and reverse ratio for DV curve.

In this work, the quantification of self-discharge is based on the approach presented by Knap et al. [58] and analyzed in Section 6.1. The proposed methodology allows to separate irreversible (battery degradation) and reversible

Table 2
Storage conditions of investigated Li-S pouch cells for calendar aging.

Temperature [°C]	DOD [%]		
	0	50	90
7.5	-	X	-
30	X	X	X
50	-	X	-

(self-discharge) capacity loss. At the end of the RPT measurement, the cell was discharged to a target DOD state and after one month of resting, at the beginning of the next RPT, the remaining capacity of the cell was fully discharged. The total loss of capacity (C_t) is expressed by subtracting the discharge capacity obtained from the DOD setting (C_{dod}) and the remaining discharge capacity (C_{rem}) from the total discharging capacity (C_{ini}) according to equation 1. The irreversible capacity loss (C_{ir}) was calculated as the difference between the capacity obtained in the previous RPT measurement and the current RPT measurement (C_{rch}) (see equation 2). The final value of self-discharge (C_{sd}) was calculated by deducting the irreversible capacity loss from the total capacity loss (see equation 3).

$$C_t = C_{sd} + C_{ir} = (C_{ini} - C_{dod} - C_{rem})/C_{ini} \cdot 100 \tag{1}$$

$$C_{ir} = (C_{ini} - C_{rch})/C_{ini} \cdot 100 \tag{2}$$

$$C_{sd} = (C_{rch} - C_{rem} - C_{dod})/C_{ini} \cdot 100 \tag{3}$$

The direct shuttle current methodology is based on the procedure presented by Knap and coworkers [60] and evaluated in Section 6.2. The Li-S cell was fully charged and rested in an open circuit condition to reach an OCV value. In the next step, the cells were held in constant voltage charging mode at the detected OCV value and the current was observed for 2 hours in order to determine the steady-state value denoted as the shuttle current.

A detailed study of internal resistance and EIS measurements is demonstrated in Section 7. The EIS measurements were performed in the frequency range from 10 kHz to 10 mHz with a voltage amplitude of 3 mV. Simulation of EIS spectra was calculated in MATLAB software using the 'Zfit' function [81]. An equivalent electrical circuit, depicted in Fig. 2, is proposed for studying the electrochemical behavior of the Li-S batteries. The applied equivalent electrical circuit and its fitting are described in detail in [82]. In this model, the constant phase element (CPE) was used instead of the capacitor due to the non-ideal behavior of the system. The electrolyte resistance is expressed by R_e and represents the contribution of ohmic resistance. The first semicircle is described by R_{int} and CPE_{int} which corresponds to interphase contact resistance and the capacitance in the sulfur electron bulk. The second semicircle is described by charge transfer resistance and the capacitance of the double layer on the electrode surface represented by R_{ct} and CPE_{dl}. The straight line at the end of spectra is described by the diffusion process and R_{diff}, CPE_{diff}, W (Warburg element) parameters.

4. Capacity Evolution

The normalized capacity as a function of time at different temperatures and 50 % of DOD is shown in Fig. 3a. As expected, cells stored at a high temperature of 50 °C cause a significant acceleration of the capacity decline. Capacity retention at high-temperature conditions was around 40 % after 15 months. After the first month of calendar aging, a significant drop in the capacity occurred for the cells stored at 7.5 °C. As a result, higher degradation was observed for the cells stored at 7.5 °C than for the cells stored at 30 °C, during the entire testing period. However, observing the long-term trend and the change in capacity throughout the observed period, it is expected that the cells stored at 30 °C would eventually achieve a larger capacity decline than the 7.5 °C stored cells. The influence of DOD on capacity decrease at 30 °C is summarized in Fig. 3b. The lowest capacity decrease during the first six months was observed for

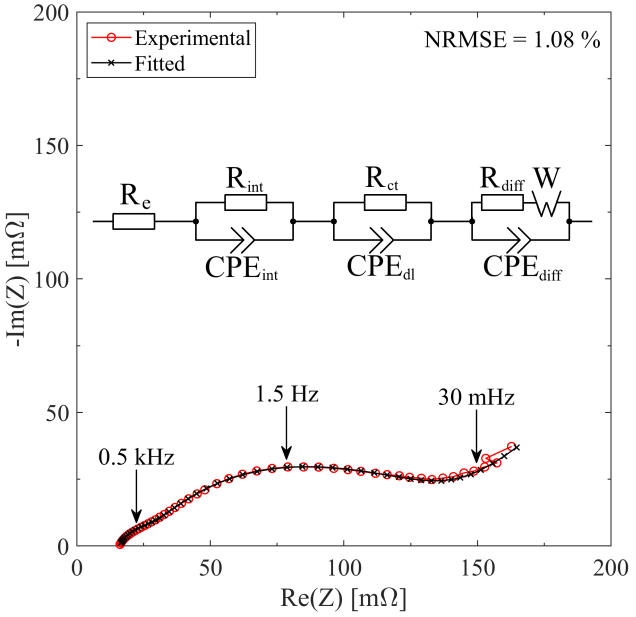

Fig. 2: Equivalent electrical circuit used for fitting the experimental EIS data and an example of Nyquist plot of the Li-S pouch cell at 15 % DOD stored at 50 °C and 50 % of DOD at the beginning of life.

the fully charged state (0 % of DOD) of the battery. After the first half of the year and until the end of the experiment the lowest capacity drop was perceived for the half-discharged cell (50 % DOD). One can see that the capacity fade for 0 and 90 % of DOD seem very similar after 10-month storage. After 2 years of storage, the dispersion of capacity values is greater for 0 % of DOD which may indicate higher instability and degradation of the material due to the presence of the shuttle effect in a fully charged state [18].

In order to better understand the capacity evolution of the Li-S cells, the discharge curves were closely examined. The evolution of the capacity arising in high and low voltage plateau at different temperatures and DODs is shown in Fig. 3c-f. The sum of the capacity from both plateaus is always equal to one and graphs represent the capacity ratio in high voltage and low voltage plateaus. It is observed that at the beginning of life, around 70 % of total capacity is associated with the low voltage plateau where the polysulfides with short-chain are formed. Fig. 3c,e presents temperature dependence of capacity calculated from high and low voltage plateau at 50 % of DOD. The high temperature of 50 °C during storage results in an initial increase of capacity in the high voltage plateau during the first five months and then capacity decreases. Low calendar aging temperature causes the capacity to increase in the high voltage plateau after the first month of storage and then the capacity continuously decreases. The reverse process was observed for the low voltage plateau, after an initial decrease, the capacity increases. The capacity variation after the first month of storage is due to a sharp drop in total capacity. The behavior of capacity in both plateaus at a storage temperature of 30 °C is more linear compared to other temperatures. The capacity rises slightly in the high voltage plateau and, conversely, decreases in the low voltage plateau. The impact of DOD level on capacity during storage at 30 °C in both plateaus is depicted in Fig. 3d,f. The scattering of capacity values in the fully charged condition (0 % DOD) is approximately ten times higher compared to cells stored in a moderate or discharged state. The capacity of the upper plateau has a declining tendency and growing movement may be observed in the lower plateau. The decline in the capacity of the cells stored at 50 and 90 % of DOD is higher in the low voltage plateau compared to the high voltage plateau. Beyond, the rate of growth or decline is greater at 90 % of DOD than 50 % of DOD. The presence of soluble higher polysulfides during storage of the cell in a fully charged state has an impact on decreasing capacity in a high voltage plateau presumably due to side reactions of dissolution of long-chain polysulfides in the electrolyte during shelf storage [83]. As the amount of higher polysulfides during shelf storage decreases, the capacity of the high voltage plateau gently decreases.

The effectiveness of charging and discharging the battery may be expressed by Coulombic efficiency. Coulombic efficiency of the analyzed Li-S pouch cells is presented in Fig. 3g,h. The cells stored at 30 °C achieve the highest

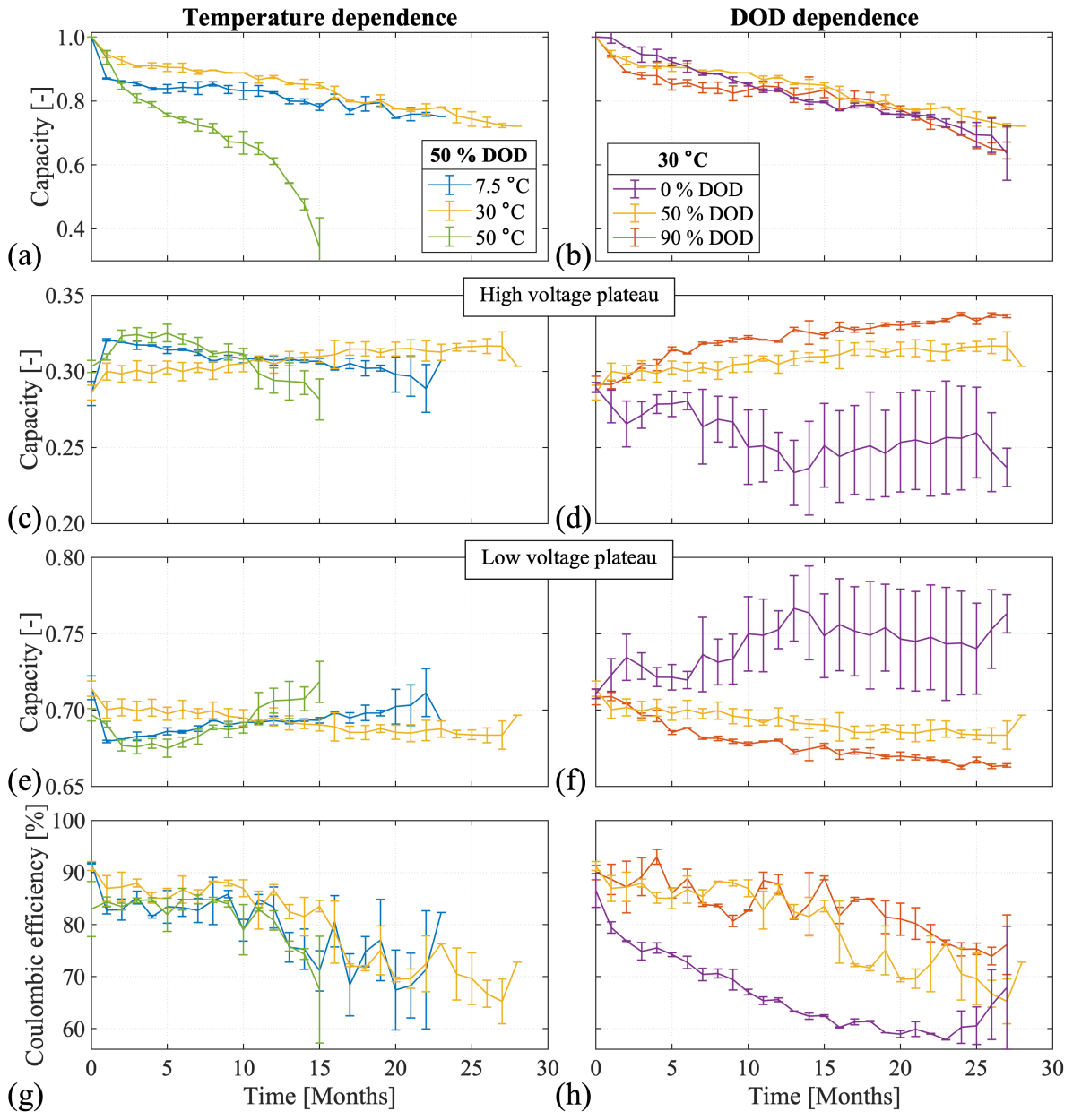

Fig. 3: Evolution of total capacity, capacities obtained from high and low voltage plateaus, and Coulombic efficiency for various temperatures and DODs.

average value of efficiency. The efficiency at high and low temperatures is slightly lower and gently decreases with time for all test cases indicating the slowly intensified impact of the shuttle effect of polysulfides [84]. However, the state of the DOD has a large impact on Coulombic efficiency. The occurrence of dissolution of higher polysulfides and shuttle (see Section 6.2) during storage in a fully charged state causes a dramatic decline in efficiency. To sum up, optimal storage conditions for Li-S batteries longevity appear to be 30 °C and DOD around 50 %.

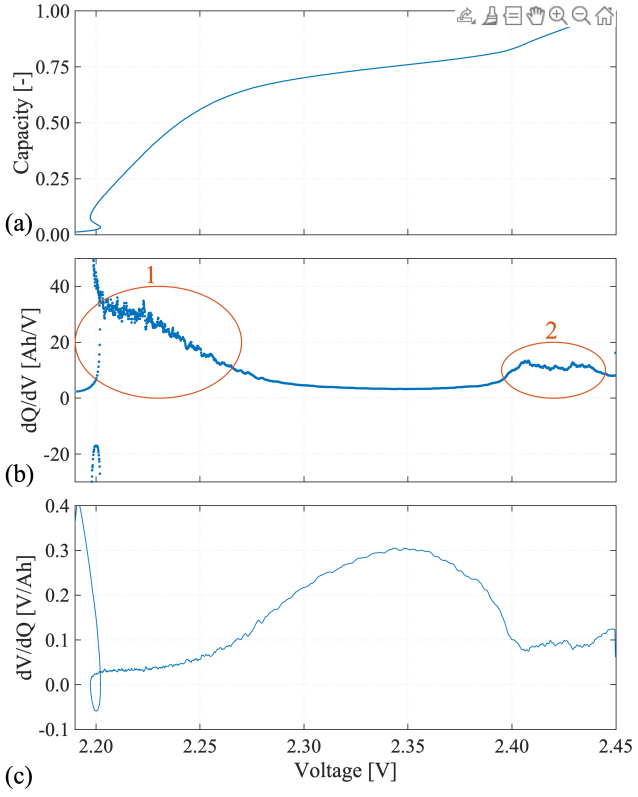

Fig. 4: Charging curve, IC and DV curves at the beginning-of-life of the Li-S cell.

5. IC and DV curves

In order to further investigate the battery changes during aging and identify the loss of active material, ICA and DVA analyses of the charge curves were performed. Both analyses were performed during charging due to easier control of the charging process than of the discharging process, during the normal real-life operation of the battery.

The charging curve at 0.1 C expressed in the inverse dependence of voltage and capacity, to easier describe processes in IC and DV curves, is shown in Fig. 4a. A typical voltage kink around 2.2 V during charging is visible.

Interpretation of the charging curves in the dQ/dV vs V plot is presented in Fig. 4b. Instead of the voltage kink, there appears a vertical line and an arc in the negative area followed by two peaks. The first peak observed around 2.21 V corresponds to the low voltage plateau where short-chain polysulfides are transformed into long-chain polysulfides. The second peak detected around 2.41 V correlate with the high voltage plateau and transformation of long-chain polysulfides to sulfur.

Plotting the inverse ratio as dV/dQ instead of dQ/dV gives us more quantifiable graphical dependencies (see Fig. 4c). The voltage kink in this form is visible as the loop and the sharp rising part between the plateaus of the curve is presented by the peak around 2.34 V which is consistent with a valley in the dQ/dV curve.

In order to analyze the result quantitatively, the peak that occurred in dV/dQ vs V dependency was fitted using the open code 'peakfit' in MATLAB [85]. Fig. 5 presents the evolution of the peak characteristics as a function of capacity at various temperatures and DODs. The peaks were considered to have the shape of Gaussian distribution to achieve the best fitting accuracy, and for each peak, quantitative information was obtained for analysis, such as the position, height, and width of the peak where the width was calculated at half the peak height.

The peak position divides the DV curve into two regions, with the first region corresponding to the low voltage plateau and the second to the high voltage plateau. The changes in the peak position with capacity decrease are depicted in Fig. 5a,b. The position of the peak is gently shifted to lower potential with a capacity decrease for 7.5 °C and 30 °C. The most significant change in a peak position was observed for 50 °C, where the peak shifted towards a higher potential with a capacity decay. The instability of the peak position agrees with the high capacity decay (Fig. 3c) and increase in

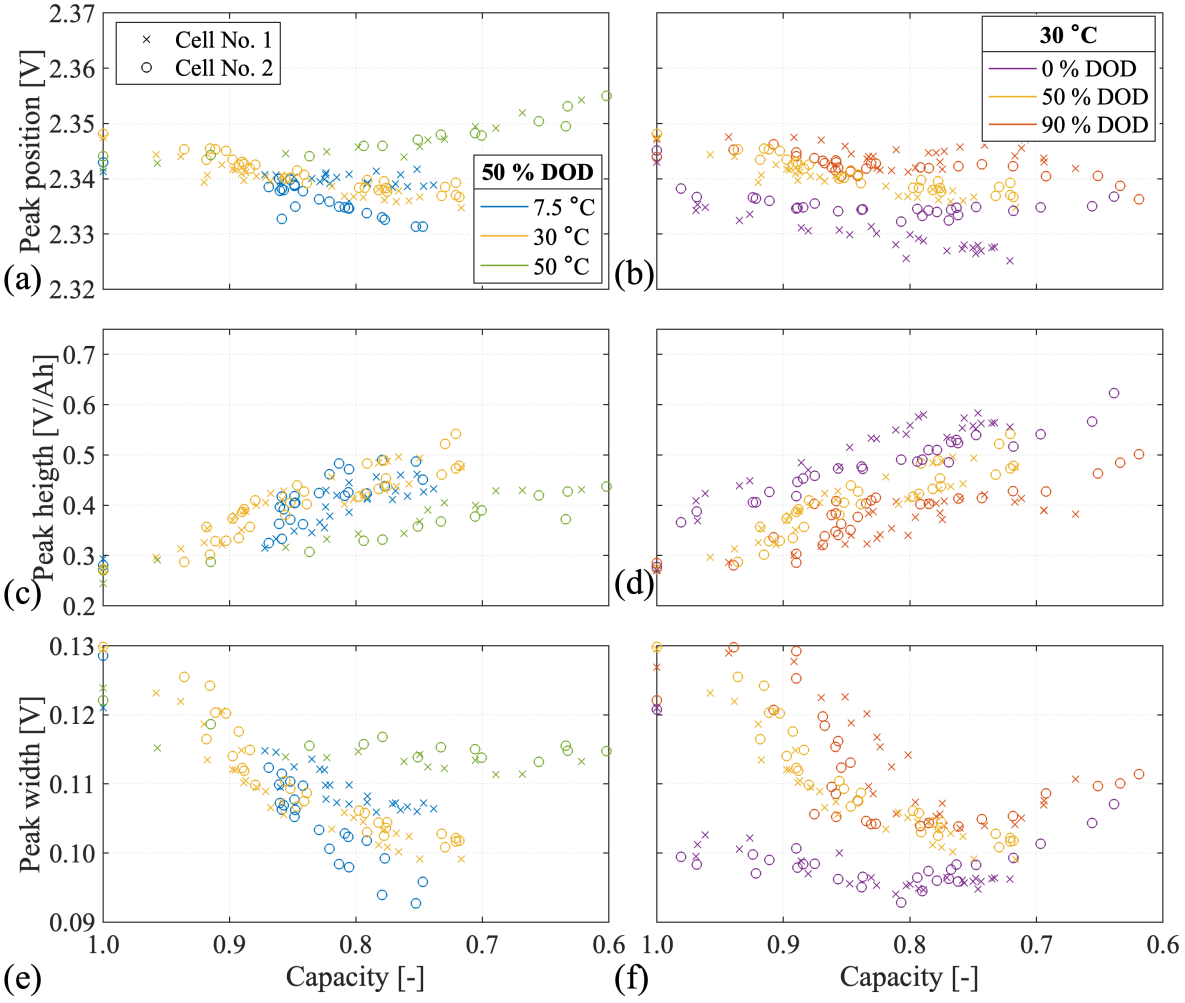

Fig. 5: Peak parameter evaluations for the cells stored at different temperatures and DODs.

resistance (Fig. 7) observed for 50 °C. The influence of the DOD storage resulted in a gentle shift of the peak to lower potential with a capacity decrease. The most significant shift of the peak position was observed at 0 % DOD.

The evolution of the peak height and width with capacity decrease is illustrated in Fig. 5c-f. The intensity of the peak increases and the peak width is shortened with capacity decay for all test cells. The highest and narrowest peaks may be observed from curves at 30 °C and 7.5 °C. The capacity decrease at 50 °C was very fast, the peaks with the lowest intensity and the broadest width are visible. A low DOD results in high peak intensity and narrow shape, conversely, a high DOD results in a low peak height with a broad profile. The peak height is in agreement with the behavior of the shuttle current (see Fig. 6d). The shuttle current increases with the peak height.

6. Evaluation of Self-Discharge and Shuttle Current

6.1. Self-Discharge

The self-discharge rate of the 3.4 Ah Li-S pouch cells at different temperatures and DODs are presented in Fig. 6a,b. A high temperature of 50 °C resulted in an increase in self-discharge compared to lower temperatures and accelerated side reactions during shelf storage. The negative value of self-discharge at the end of the experiment at high temperature is due to a dramatic decrease in capacity (see Fig. 3a). The self-discharge rate at 30 and 7.5 °C is stable up to one year of storage and exhibits a negative value which may be a sign of the capacity recovery effect [86, 87]. Monotonous

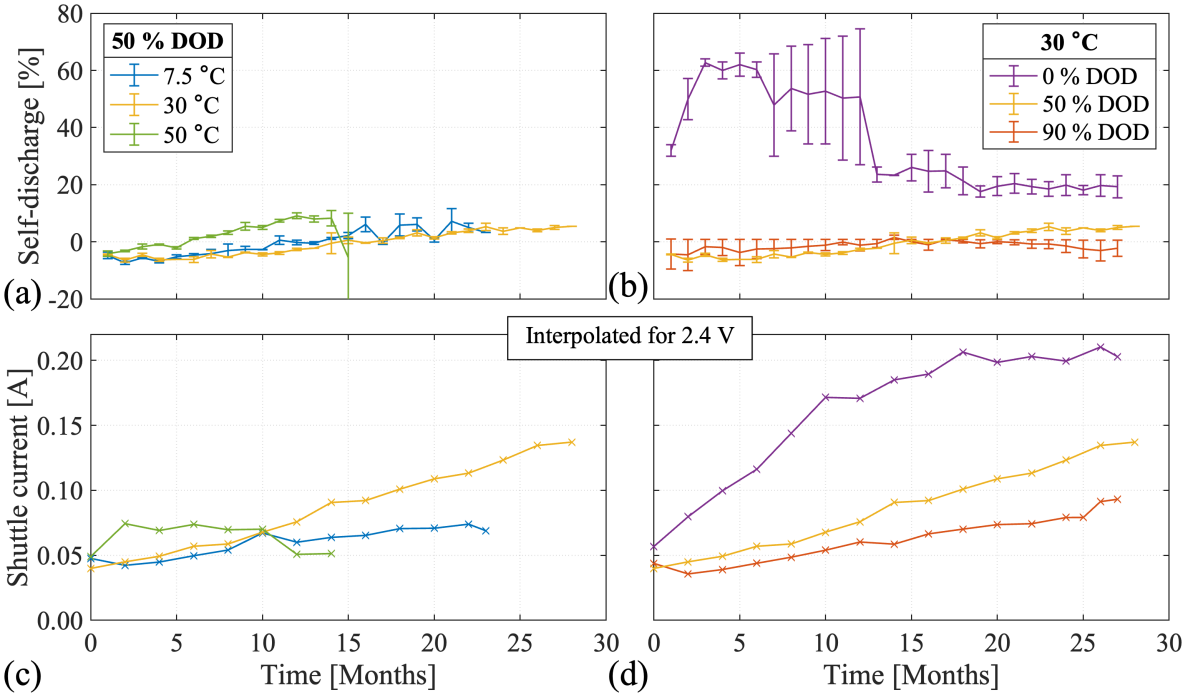

Fig. 6: Self-discharge rate and shuttle current value interpolated for 2.4 V at different temperatures and DODs.

gentle increase of self-discharge up to ~5 % takes place due to dissolution of higher polysulfides during battery resting and chemical reactions on the anode surface [44, 56, 88].

The self-discharge behavior of the Li-S batteries stored at different DODs as a function of time is presented in Fig. 6b. As expected, the self-discharge rate for cells stored at 0 % DOD was around 30 % after the first month of calendar aging. The self-discharge rate further increased during the first year of the calendar aging up to 50 - 60 % and then stabilized around 20 %. The main reason for the capacity loss is due to the reduction of the high voltage plateau capacity to almost zero. The increase in self-discharge may be caused by the dissolution of polysulfides, an increase of shuttle, and unsatisfactory charging in the previous cycle, respectively [89]. The decrease in self-discharge may be caused by material stabilization and recovery of sulfur and polysulfides during cycling. The self-discharge rate for the cells stored at 50 and 90 % of DOD is small, not exceeding 5 % during the whole aging test period. The side reactions of higher polysulfides during the shelf storage increase the rate of self-discharge [90].

6.2. Shuttle Current

The interpolated value of shuttle current for 2.4 V is presented in Fig. 6c,d. The presence of high temperature accelerates side reactions in Li-S batteries. The temperature of 50 °C causes the highest value of shuttle current in the first 10 months, then the cells reached the critical capacity (see Fig. 3a), and their end of life was reached. The impact of DOD on shuttle current is illustrated in Fig. 6d. The shuttle current increases with decreasing of DOD storage and its evolution confirms the tendency of Coulombic efficiency (see Fig. 3h). The increase of shuttle current with storage time indicates a higher amount of soluble polysulfides in the electrolyte [91].

7. Internal Resistance and EIS

In order to analyze the evolution of the resistance during the degradation of the battery, the measurement of internal resistance by current pulses was performed. The resistance determined for one second discharging by a current pulse of 0.2 C is illustrated in Fig. 7 at 10 and 70 % of DOD representing high and low voltage plateau and various shelf storage conditions (temperature and storage DOD). The value of resistance is higher for the low voltage plateau, due to the formation of lower-order polysulfides which is in an agreement with the results in [92]. With the increasing storage

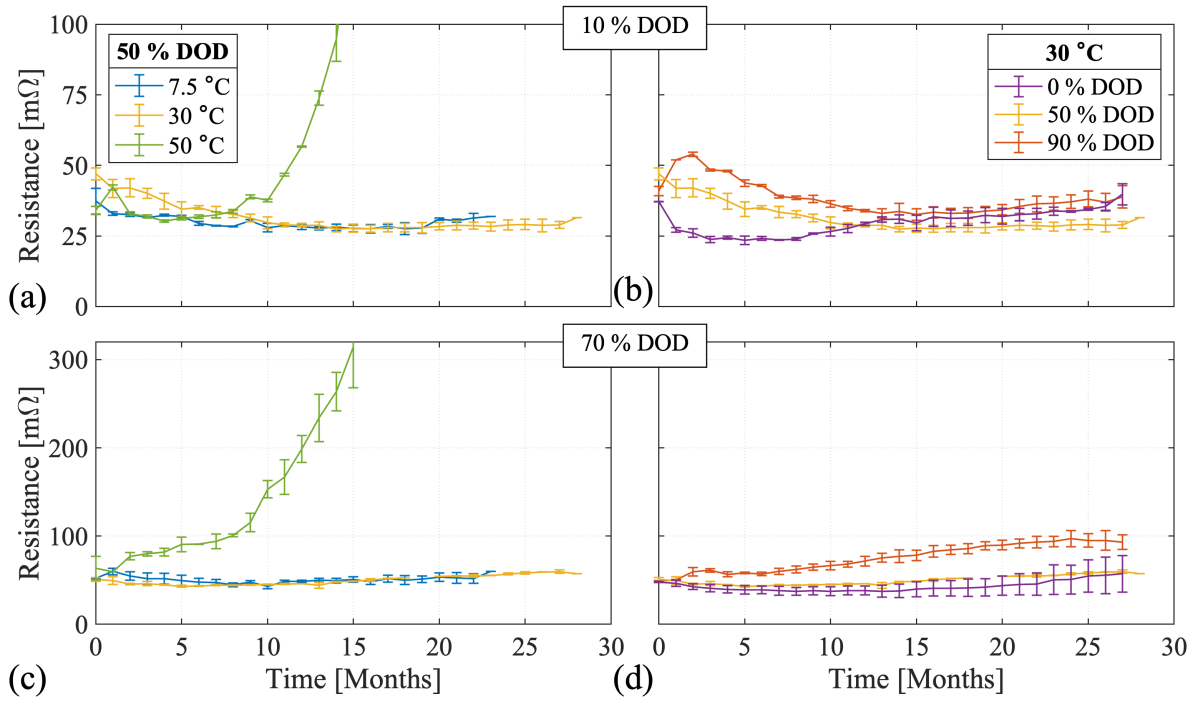

Fig. 7: Measured resistance for a 1-second discharge with a 0.2 C current at different DODs for various conditions.

time, the resistance increases for 50 °C as a result of accelerated degradation of the material. The resistance evolution for 30 and 7.5 °C is stable or has a gently declining trend. Concerning the storage DOD level, the highest resistance is observed for discharge state conditions (90 % DOD) in both plateaus and during the whole time of storage. This phenomenon may be linked to the presence of non-conductive discharge products (Li_2S_2, Li_2S), their precipitation, and the formation of the passivation layer in a discharged state during storage [93]. The resistance at the storage of 50 % DOD has a decreasing trend with time at 10 % DOD. Contrary, storage at 0 % DOD results in a slight increase of the resistance. The evolution of resistance in the low voltage plateau under storage conditions of 50 and 0 % DOD is similar with increasing tendency.

The EIS characterization was performed at different values of DOD during the RPT procedure. Here we analyze the EIS spectra at 15 and 70 % DOD to compare resistances from high and low voltage plateaus, similar to the measured internal resistance from the current pulses. The effect of the aging conditions at different temperatures and DODs on calculated resistances is illustrated in Fig. 8. The resistance obtained from current pulses is higher in the low voltage plateau and the same behavior was observed for calculated resistance from EIS measurements. The evolution of the resistances with time is analyzed over two years. Although, the last EIS measurement for the Li-S battery stored at 50 °C was performed in the eighth month of storage due to fast capacity decay.

The electrolyte resistance R_e (blue line in Fig. 8) in both plateaus has a gently rising tendency. The presence of higher polysulfides in the electrolyte increases the viscosity and the result is a higher increase of electrolyte resistance in high voltage plateau than in low voltage plateau. The resistance is increasing with time due to the gradually increasing amount of polysulfides in the electrolyte [94]. One can see that the electrolyte resistance increases slightly with increasing temperature at the end of the storage time. The behavior of the electrolyte resistance in the low voltage plateau at different DOD conditions seems fairly stable. However, storage of the cell in a charged state with long-chain polysulfides has resulted in an increase in electrolyte resistance.

The interphase contact resistance R_{int} (orange line in Fig. 8) is stable up to approximately 12 months of storage and then increases in all cases as a result of the presence of cracks in the cathode material. The resistance values drop in the low voltage plateau indicating improved interfacial contact between sulfur particles due to composition changes of the cathode. The increase of electrode/electrolyte resistance in high voltage plateau may be a result of the formation of longer chain polysulfides in the electrode pores [75]. The observed effect of storage temperature on R_{int} is relatively

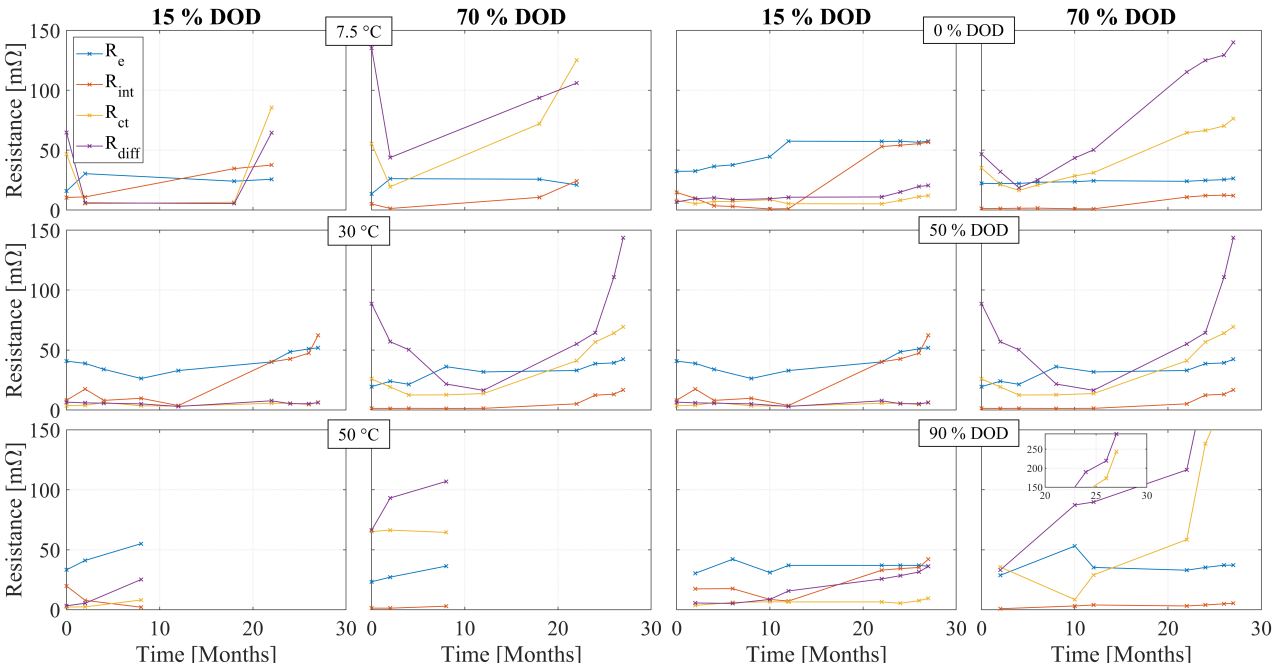

Fig. 8: Calculated resistances and their evolution in a high and low voltage plateau at various temperature levels at 50 % DOD (left side) and different DOD levels at 30 °C (right side).

small with an increasing trend for lower temperatures, at the end of the experiment. The higher amount of long-chain polysulfides during storage increased R_{int} in high voltage plateau after 20 months of shelf storage. The lower plateau shows quite stable resistance concerning different DOD values during storage.

The charge transfer resistance R_{ct} is lower in the high voltage plateau than in the low voltage plateau as a result of the sulfur reduction to long-chain polysulfides suggesting fast reaction kinetics in high voltage plateau. The increase of R_{ct} in the low voltage plateau may cause a slower reduction of higher polysulfides resulting in less soluble polysulfides (Li_2S_2 and Li_2S) and the creation of an insoluble layer. The charge transfer resistance in the low voltage plateau increases with time due to the presence of a higher amount of less soluble Li_2S_2, Li_2S, and a growing insoluble layer [95]. The charge transfer resistance reached the highest value at the lowest temperature in the low voltage plateau. Concerning the storage DOD level, the charge transfer resistance in the low voltage plateau increases with higher DOD and the formation of short-chain polysulfides and a passivation layer.

A blocking layer continues to deposit on the cathode surface from poorly soluble short chain polysulfides which are described by diffusion resistance [96]. The diffusion resistance R_{diff} is lower in high voltage plateau than in low voltage plateau as a result of a large amount of long-chain polysulfides where the diffusion resistance is suppressed. Contrary, R_{diff} has higher values in the low voltage plateau due to the presence of short-chain polysulfides and the formation of a blocking layer on the electrode surface [94]. The resistance in low voltage plateau may decrease for the first months due to oxidation of a larger amount of short-chain polysulfides and thinning of the blocking layer on the cathode. The subsequent increase may be related to a higher amount of insoluble lower polysulfides in the electrolyte, which have insulating properties and increase the thickness of the deposition layer on the cathode. No dependence of storage temperature on diffusion resistance is evident from our results. Formation of a blocking layer during storage in a discharged state resulted in the highest R_{diff} in the low voltage plateau.

8. Conclusions

Most of the research on Li-S batteries has focused on cycling aging, therefore more emphasis needs to be focused on the investigation of calendar aging to determine ideal storage conditions. Furthermore, calendar aging cannot be straightforwardly separated from cycling aging. However, to accelerate the successful commercialization of Li-S batteries, storage conditions need to be optimized on a large scale and not just on a lab-scale (coin cells, hand-made

pouch cells with capacities below 1 Ah), due to the fact that some phenomena are only observed on a large scale (pre-commercial or commercial pouch cells with capacities higher than 1 Ah). To the best of the authors' knowledge, the calendar life of Li-S batteries has so far been observed only under a single condition, on a small scale, and/or mostly over a short period of time, while this work addresses all of these deficiencies.

The degradation behavior of pre-commercial 3.4 Ah Li-S pouch cells was thoroughly analyzed during long-term shelf storage by non-destructive characterization techniques. To extend the analysis, the Li-S cells were stored under various conditions, at three temperature levels (7.5, 30, and 50 °C) and three DOD states (0, 50, and 90 %). The capacity fade during calendar aging results from side reactions that reduce the sulfur inventory. The most significant side reaction is the shuttle effect, the presence of which is clearly visible during storage in the fully charged state in the rapid capacity decay at high voltage plateau and high shuttle current. The high temperature may decrease the activation energy of the reaction which results in accelerated side reaction rate and diffusion. A deeper DVA analysis is used for the first time to study the calendar aging of Li-S batteries. The peak characteristics can help to determine the state-of-health of the battery.

Calendar aging of Li-S batteries in practical applications may be reduced by storage at low temperature and high DOD. The DOD state should remain higher than 30 %, which represents the capacity of a high voltage plateau. This avoids storage at high potential, where higher-order polysulfides are formed and involved in the shuttle effect. Storage at low DOD causes a high self-discharge rate (in the early stage up to 70 % and stabilized around 20 % after 27 months), high shuttle current (up to 0.2 A), low Coulombic efficiency (dropping down to 60 %), and accelerated capacity loss. The high temperature accelerates the side reactions and after a short period of time, there is a significant drop in capacity. Moreover, the increase of the resistance was observed during storage in a discharged state in a low voltage plateau, due to the formation of a passivation layer from non-conductive discharge products (Li_2S_2, Li_2S).

The tracking of the calendar aging and its diagnosis is very time-consuming. The development of rapid tests to reliably assess the long-term stability of cells could be critical to the implementation of Li-S in the battery industry. The analysis of the Li-S pouch cells may be enhanced by measuring volume changes during the experiments and investigating the effect of pressure on cell properties.

Acknowledgments

The authors would like to thank OXIS Energy for supplying the Lithium–Sulfur battery cells. This work was supported by the Ministry of Education, Science, Research and Sport of the Slovak Republic under project No. 313011V334, Innovative Solutions for Propulsion, Power and Safety Components of Transport Vehicles and the Operational Programme Integrated Infrastructure for the project: Regeneration of used batteries from electric vehicles, ITMS2014+: 313012BUN5, which is part of the Important Project of Common European Interest (IPCEI), called European Battery Innovation in the Operational Program Integrated Infrastructure, call code: OPII-MH/DP/2021/9.5-34, co-financed from the resources of the European Regional Development Fund.

CRediT authorship contribution statement

Dominika Capkova: Data curation, Writing - Original draft preparation. **Vaclav Knap:** Data curation, Conceptualization of this study, Methodology, Supervision, Writing - Reviewing and Editing. **Andrea Strakova Fedorkova:** Writing - Reviewing and Editing. **Daniel-Ioan Stroe:** Methodology, Supervision, Writing - Reviewing and Editing.

References

[1] A. Manthiram, Y. Fu, Y.-S. Su, Challenges and prospects of lithium–sulfur batteries, Accounts of Chemical Research 46 (5) (2012) 1125–1134. doi:10.1021/ar300179v.

[2] M. Zhao, B.-Q. Li, H.-J. Peng, H. Yuan, J.-Y. Wei, J.-Q. Huang, Lithium–sulfur batteries under lean electrolyte conditions: Challenges and opportunities, Angewandte Chemie International Edition 59 (31) (2020) 12636–12652. doi:10.1002/anie.201909339.

[3] L. Chladil, D. Kunický, T. Kazda, P. Vanýsek, O. Čech, P. Bača, In-situ XRD study of a chromium doped LiNi0.5mn1.5o4 cathode for li-ion battery, Journal of Energy Storage 41 (2021) 102907. doi:10.1016/j.est.2021.102907.

[4] L. Chladil, D. Kunický, P. Vanýsek, O. Čech, In-situ x-ray study of carbon coated LiFePO4 for li-ion battery in different state of charge, ECS Transactions 87 (1) (2018) 107–114. doi:10.1149/08701.0107ecst.

[5] G. Ye, M. Zhao, L.-P. Hou, W.-J. Chen, X.-Q. Zhang, B.-Q. Li, J.-Q. Huang, Evaluation on a 400 wh kg-1 lithium–sulfur pouch cell, Journal of Energy Chemistry 66 (2022) 24–29. doi:10.1016/j.jechem.2021.07.010.

[6] T. Kazda, M. Krbal, M. Pouzar, J. Vondrák, A. F. Straková, M. Slávik, T. Wagner, J. Macak, Highly efficient and stable cryo-ground sulphur cathode for li-s batteries, Journal of Power Sources 331 (2016) 293–298. doi:10.1016/j.jpowsour.2016.09.050.

[7] O. Cech, P. Vanysek, L. Chladil, K. Castkova, Mixed sodium titanate as an anode for a sodium-ion battery, ECS Transactions 74 (1) (2016) 331–337. doi:10.1149/07401.0331ecst.

[8] D. Capkova, T. Kazda, P. Čudek, A. S. Fedorkova, Binder influence on electrochemical properties of li-s batteries, ECS Transactions 99 (1) (2020) 161–167. doi:10.1149/09901.0161ecst.

[9] S.-H. Chung, L. Luo, A. Manthiram, TiS2–polysulfide hybrid cathode with high sulfur loading and low electrolyte consumption for lithium–sulfur batteries, ACS Energy Letters 3 (3) (2018) 568–573. doi:10.1021/acsenergylett.7b01321.

[10] T. Kazda, D. Capková, K. Jaššo, A. F. Straková, E. Shembel, A. Markevich, M. Sedlaříková, Carrageenan as an ecological alternative of polyvinylidene difluoride binder for li-s batteries, Materials 14 (19) (2021) 5578. doi:10.3390/ma14195578.

[11] D. Capková, M. Almáši, T. Kazda, O. Čech, N. Király, P. Čudek, A. S. Fedorková, V. Hornebecq, Metal-organic framework MIL-101(fe)–NH2 as an efficient host for sulphur storage in long-cycle li–s batteries, Electrochimica Acta 354 (2020) 136640. doi:10.1016/j.electacta.2020.136640.

[12] Y. Xie, H. Zhao, H. Cheng, C. Hu, W. Fang, J. Fang, J. Xu, Z. Chen, Facile large-scale synthesis of core–shell structured sulfur@polypyrrole composite and its application in lithium–sulfur batteries with high energy density, Applied Energy 175 (2016) 522–528. doi:https://doi.org/10.1016/j.apenergy.2016.03.085.
URL https://www.sciencedirect.com/science/article/pii/S0306261916304111

[13] S. Waluś, G. Offer, I. Hunt, Y. Patel, T. Stockley, J. Williams, R. Purkayastha, Volumetric expansion of lithium-sulfur cell during operation – fundamental insight into applicable characteristics, Energy Storage Materials 10 (2018) 233–245. doi:10.1016/j.ensm.2017.05.017.

[14] S. S. Zhang, Liquid electrolyte lithium/sulfur battery: Fundamental chemistry, problems, and solutions, Journal of Power Sources 231 (2013) 153–162. doi:10.1016/j.jpowsour.2012.12.102.

[15] D. Capkova, T. Kazda, O. Petruš, J. Macko, K. Jasso, A. Baskevich, E. Shembel, A. S. Fedorkova, Pyrite as a low-cost additive in sulfur cathode material for stable cycle performance, ECS Transactions 105 (1) (2021) 191–198. doi:10.1149/10501.0191ecst.

[16] T. Kazda, P. Čudek, J. Vondrák, M. Sedlaříková, J. Tichý, M. Slávik, G. Fafilek, O. Čech, Lithium-sulphur batteries based on biological 3d structures, Journal of Solid State Electrochemistry 22 (2) (2017) 537–546. doi:10.1007/s10008-017-3791-0.

[17] D. Skoda, T. Kazda, L. Munster, B. Hanulikova, A. Styskalik, P. Eloy, D. P. Debecker, P. Vyroubal, L. Simonikova, I. Kuritka, Microwave-assisted synthesis of a manganese metal–organic framework and its transformation to porous MnO/carbon nanocomposite utilized as a shuttle suppressing layer in lithium–sulfur batteries, Journal of Materials Science 54 (22) (2019) 14102–14122. doi:10.1007/s10853-019-03871-4.

[18] Y. V. Mikhaylik, J. R. Akridge, Polysulfide shuttle study in the li/s battery system, Journal of The Electrochemical Society 151 (11) (2004) A1969. doi:10.1149/1.1806394.

[19] Y. Li, J. Wu, B. Zhang, W. Wang, G. Zhang, Z. W. Seh, N. Zhang, J. Sun, L. Huang, J. Jiang, J. Zhou, Y. Sun, Fast conversion and controlled deposition of lithium (poly)sulfides in lithium-sulfur batteries using high-loading cobalt single atoms, Energy Storage Materials 30 (2020) 250–259. doi:10.1016/j.ensm.2020.05.022.

[20] L. Li, Z. P. Wu, H. Sun, D. Chen, J. Gao, S. Suresh, P. Chow, C. V. Singh, N. Koratkar, A foldable lithium–sulfur battery, ACS Nano 9 (11) (2015) 11342–11350. doi:10.1021/acsnano.5b05068.

[21] X. Ji, K. T. Lee, L. F. Nazar, A highly ordered nanostructured carbon–sulphur cathode for lithium–sulphur batteries, Nature Materials 8 (6) (2009) 500–506. doi:10.1038/nmat2460.

[22] Q. Lu, Y. Zhong, W. Zhou, K. Liao, Z. Shao, Dodecylamine-induced synthesis of a nitrogen-doped carbon comb for advanced lithium-sulfur battery cathodes, Advanced Materials Interfaces 5 (9) (2018) 1701659. doi:10.1002/admi.201701659.

[23] D. Capková, T. Kazda, A. S. Fedorková, P. Čudek, R. Oriňaková, Carbon materials as the matrices for sulfur in li-s batteries, ECS Transactions 95 (1) (2019) 19–26. doi:10.1149/09501.0019ecst.

[24] M.-Q. Zhao, Q. Zhang, J.-Q. Huang, G.-L. Tian, J.-Q. Nie, H.-J. Peng, F. Wei, Unstacked double-layer templated graphene for high-rate lithium–sulphur batteries, Nature Communications 5 (1) (mar 2014). doi:10.1038/ncomms4410.

[25] G. Zhou, S. Pei, L. Li, D.-W. Wang, S. Wang, K. Huang, L.-C. Yin, F. Li, H.-M. Cheng, A graphene-pure-sulfur sandwich structure for ultrafast, long-life lithium-sulfur batteries, Advanced Materials 26 (4) (2013) 625–631. doi:10.1002/adma.201302877.

[26] Z. W. Lu, Y. H. Wang, Z. Dai, X. P. Li, C. Y. Zhang, G. Z. Sun, C. S. Gong, X. J. Pan, W. Lan, J. Y. Zhou, E. Q. Xie, One-pot sulfur-containing ion assisted microwave synthesis of reduced graphene oxide@nano-sulfur fibrous hybrids for high-performance lithium-sulfur batteries, Electrochimica Acta 325 (2019) 134920. doi:10.1016/j.electacta.2019.134920.

[27] F. Liu, J. Liang, C. Zhang, L. Yu, J. Zhao, C. Liu, Q. Lan, S. Chen, Y.-C. Cao, G. Zheng, Reduced graphene oxide encapsulated sulfur spheres for the lithium-sulfur battery cathode, Results in Physics 7 (2017) 250–255. doi:10.1016/j.rinp.2016.12.049.

[28] R. Demir-Cakan, M. Morcrette, F. Nouar, C. Davoisne, T. Devic, D. Gonbeau, R. Dominko, C. Serre, G. Férey, J.-M. Tarascon, Cathode composites for li–s batteries via the use of oxygenated porous architectures, Journal of the American Chemical Society 133 (40) (2011) 16154–16160. doi:10.1021/ja2062659.

[29] J. Ge, L. Fan, A. M. Rao, J. Zhou, B. Lu, Surface-substituted prussian blue analogue cathode for sustainable potassium-ion batteries, Nature Sustainability (3) (2021) 225–234.

[30] Y. Hu, L. Fan, A. M. Rao, W. Yu, C. Zhuoma, Y. Feng, Z. Qin, J. Zhou, B. Lu, Cyclic-anion salt for high-voltage stable potassium-metal batteries, National Science Review 9 (10) (jul 2022). doi:10.1093/nsr/nwac134.

[31] C. Shi, S. Shao, C. Zong, J. Gu, Z. Huang, B. Hong, M. Wang, Z. Zhang, Y. Lai, J. Li, Organothiols for dual-interface modification of high performance lithium-sulfur batteries, Chemical Engineering Journal 448 (2022) 137552. doi:10.1016/j.cej.2022.137552.

[32] X.-B. Cheng, R. Zhang, C.-Z. Zhao, Q. Zhang, Toward safe lithium metal anode in rechargeable batteries: A review, Chemical Reviews 117 (15) (2017) 10403–10473. doi:10.1021/acs.chemrev.7b00115.

[33] S. Li, H. Dai, Y. Li, C. Lai, J. Wang, F. Huo, C. Wang, Designing li-protective layer via SOCl2 additive for stabilizing lithium-sulfur battery, Energy Storage Materials 18 (2019) 222–228. doi:10.1016/j.ensm.2018.09.012.

[34] N. Akhtar, X. Sun, M. Y. Akram, F. Zaman, W. Wang, A. Wang, L. Chen, H. Zhang, Y. Guan, Y. Huang, A gelatin-based artificial SEI for lithium deposition regulation and polysulfide shuttle suppression in lithium-sulfur batteries, Journal of Energy Chemistry 52 (2021) 310–317. doi:10.1016/j.jechem.2020.04.046.

[35] S. Xiong, K. Xie, Y. Diao, X. Hong, Properties of surface film on lithium anode with LiNO3 as lithium salt in electrolyte solution for lithium–sulfur batteries, Electrochimica Acta 83 (2012) 78–86. doi:10.1016/j.electacta.2012.07.118.

[36] X. Liang, Z. Wen, Y. Liu, M. Wu, J. Jin, H. Zhang, X. Wu, Improved cycling performances of lithium sulfur batteries with LiNO3-modified electrolyte, Journal of Power Sources 196 (22) (2011) 9839–9843. doi:10.1016/j.jpowsour.2011.08.027.

[37] H. Pan, K. S. Han, M. H. Engelhard, R. Cao, J. Chen, J.-G. Zhang, K. T. Mueller, Y. Shao, J. Liu, Addressing passivation in lithium-sulfur battery under lean electrolyte condition, Advanced Functional Materials 28 (38) (2018) 1707234. doi:10.1002/adfm.201707234.

[38] G. Zhou, E. Paek, G. S. Hwang, A. Manthiram, Long-life li/polysulphide batteries with high sulphur loading enabled by lightweight three-dimensional nitrogen/sulphur-codoped graphene sponge, Nature Communications 6 (1) (jul 2015). doi:10.1038/ncomms8760.

[39] X.-F. Liu, H. Chen, R. Wang, S.-Q. Zang, T. C. W. Mak, Cationic covalent-organic framework as efficient redox motor for high-performance lithium-sulfur batteries, Small 16 (34) (2020) 2002932. doi:10.1002/smll.202002932.

[40] M. Mačák, P. Vyroubal, T. Kazda, K. Jaššo, Numerical investigation of lithium-sulfur batteries by cyclic voltammetry, Journal of Energy Storage 27 (2020) 101158. doi:10.1016/j.est.2019.101158.

[41] T. Cleaver, P. Kovacik, M. Marinescu, T. Zhang, G. Offer, Perspective commercializing lithium sulfur batteries: Are we doing the right research?, Journal of The Electrochemical Society 165 (1) (2017) A6029–A6033. doi:10.1149/2.0071801jes.

[42] M. Broussely, P. Biensan, F. Bonhomme, P. Blanchard, S. Herreyre, K. Nechev, R. Staniewicz, Main aging mechanisms in li ion batteries, Journal of Power Sources 146 (1-2) (2005) 90–96. doi:10.1016/j.jpowsour.2005.03.172.

[43] J. Vetter, P. Novák, M. Wagner, C. Veit, K.-C. Möller, J. Besenhard, M. Winter, M. Wohlfahrt-Mehrens, C. Vogler, A. Hammouche, Ageing mechanisms in lithium-ion batteries, Journal of Power Sources 147 (1-2) (2005) 269–281. doi:10.1016/j.jpowsour.2005.01.006.

[44] S.-H. Chung, A. Manthiram, Lithiu-sulfur batteries with the lowest self-discharge and the longest shelf life, ACS Energy Letters 2 (5) (2017) 1056–1061. doi:10.1021/acsenergylett.7b00245.

[45] B. Balagopal, C. S. Huang, M.-Y. Chow, Effect of calendar ageing on SEI growth and its impact on electrical circuit model parameters in lithium ion batteries, in: 2018 IEEE International Conference on Industrial Electronics for Sustainable Energy Systems (IESES), IEEE, 2018. doi:10.1109/ieses.2018.8349846.

[46] I. Bloom, B. Cole, J. Sohn, S. Jones, E. Polzin, V. Battaglia, G. Henriksen, C. Motloch, R. Richardson, T. Unkelhaeuser, D. Ingersoll, H. Case, An accelerated calendar and cycle life study of li-ion cells, Journal of Power Sources 101 (2) (2001) 238–247. doi:10.1016/s0378-7753(01)00783-2.

[47] D. T. Boyle, W. Huang, H. Wang, Y. Li, H. Chen, Z. Yu, W. Zhang, Z. Bao, Y. Cui, Corrosion of lithium metal anodes during calendar ageing and its microscopic origins, Nature Energy 6 (5) (2021) 487–494. doi:10.1038/s41560-021-00787-9.

[48] T. Bank, J. Feldmann, S. Klamor, S. Bihn, D. U. Sauer, Extensive aging analysis of high-power lithium titanate oxide batteries: Impact of the passive electrode effect, Journal of Power Sources 473 (2020) 228566. doi:10.1016/j.jpowsour.2020.228566.

[49] S. Thieme, J. Bruckner, A. Meier, I. Bauer, K. Gruber, J. Kaspar, A. Helmer, H. Althues, M. Schmuck, S. Kaskel, A lithium-sulfur full cell with ultralong cycle life: influence of cathode structure and polysulfide additive, Journal of Materials Chemistry A 3 (7) (2015) 3808–3820. doi:10.1039/c4ta06748g.

[50] C. Yan, X.-B. Cheng, C.-Z. Zhao, J.-Q. Huang, S.-T. Yang, Q. Zhang, Lithium metal protection through in-situ formed solid electrolyte interphase in lithium-sulfur batteries: The role of polysulfides on lithium anode, Journal of Power Sources 327 (2016) 212–220. doi:10.1016/j.jpowsour.2016.07.056.

[51] X. Chen, T.-Z. Hou, B. Li, C. Yan, L. Zhu, C. Guan, X.-B. Cheng, H.-J. Peng, J.-Q. Huang, Q. Zhang, Towards stable lithium-sulfur batteries: Mechanistic insights into electrolyte decomposition on lithium metal anode, Energy Storage Materials 8 (2017) 194–201. doi:10.1016/j.ensm.2017.01.003.

[52] N. Shateri, D. J. Auger, A. Fotouhi, J. Brighton, An experimental study on prototype lithium-sulfur cells for aging analysis and state-of-health estimation, IEEE Transactions on Transportation Electrification 7 (3) (2021) 1324–1338. doi:10.1109/tte.2021.3059738.

[53] E. Kuzmina, E. Karaseva, A. Ivanov, V. Kolosnitsyn, On the factors affecting aging and self-discharge of lithium-sulfur cells. effect of positive electrode composition, Energy Technology 7 (12) (2019) 1900134. doi:10.1002/ente.201900134.

[54] V. Knap, D. I. Stroe, Experimental study on calendaristic degradation and self-discharge of 3.4 ah lithium-sulfur pouch cells, ECS Transactions 85 (13) (2018) 267–273. doi:10.1149/08513.0267ecst.

[55] S. Gohari, V. Knap, M. R. Yaftian, Investigation on cycling and calendar aging processes of 3.4 ah lithium-sulfur pouch cells, Sustainability 13 (16) (2021) 9473. doi:10.3390/su13169473.

[56] H. Ryu, H. Ahn, K. Kim, J. Ahn, K. Cho, T. Nam, Self-discharge characteristics of lithium/sulfur batteries using TEGDME liquid electrolyte, Electrochimica Acta 52 (4) (2006) 1563–1566. doi:10.1016/j.electacta.2006.01.086.

[57] W. Li, Y. Pang, T. Zhu, Y. Wang, Y. Xia, A gel polymer electrolyte based lithium-sulfur battery with low self-discharge, Solid State Ionics 318 (2018) 82–87. doi:10.1016/j.ssi.2017.08.018.

[58] V. Knap, D.-I. Stroe, M. Swierczynski, R. Teodorescu, E. Schaltz, Investigation of the self-discharge behavior of lithium-sulfur batteries, Journal of The Electrochemical Society 163 (6) (2016) A911–A916. doi:10.1149/2.0641606jes.

[59] D. Moy, A. Manivannan, S. R. Narayanan, Direct measurement of polysulfide shuttle current: A window into understanding the performance of lithium-sulfur cells, Journal of The Electrochemical Society 162 (1) (2014) A1–A7. doi:10.1149/2.0181501jes.

[60] V. Knap, D.-I. Stroe, M. Swierczynski, R. Purkayastha, K. Propp, R. Teodorescu, E. Schaltz, A self-discharge model of lithium-sulfur batteries based on direct shuttle current measurement, Journal of Power Sources 336 (2016) 325–331. doi:10.1016/j.jpowsour.2016.10.087.

[61] M. Dubarry, V. Svoboda, R. Hwu, B. Y. Liaw, Incremental capacity analysis and close-to-equilibrium OCV measurements to quantify capacity fade in commercial rechargeable lithium batteries, Electrochemical and Solid-State Letters 9 (10) (2006) A454. doi:10.1149/1.2221767.

[62] L. Zheng, J. Zhu, D. D.-C. Lu, G. Wang, T. He, Incremental capacity analysis and differential voltage analysis based state of charge and capacity estimation for lithium-ion batteries, Energy 150 (2018) 759–769. doi:10.1016/j.energy.2018.03.023.

[63] D. Ansean, V. M. Garcia, M. Gonzalez, C. Blanco-Viejo, J. C. Viera, Y. F. Pulido, L. Sanchez, Lithium-ion battery degradation indicators via incremental capacity analysis, IEEE Transactions on Industry Applications 55 (3) (2019) 2992–3002. doi:10.1109/tia.2019.2891213.

[64] C. Pastor-Fernandez, W. D. Widanage, J. Marco, M.-A. Gama-Valdez, G. H. Chouchelamane, Identification and quantification of ageing mechanisms in lithium-ion batteries using the EIS technique, in: 2016 IEEE Transportation Electrification Conference and Expo (ITEC), IEEE, 2016. doi:10.1109/itec.2016.7520198.

[65] L. Wang, J. Liu, S. Yuan, Y. Wang, Y. Xia, To mitigate self-discharge of lithium–sulfur batteries by optimizing ionic liquid electrolytes, Energy & Environmental Science 9 (1) (2016) 224–231. doi:10.1039/c5ee02837j.

[66] A. Zimmerman, Self-discharge losses in lithium-ion cells, IEEE Aerospace and Electronic Systems Magazine 19 (2) (2004) 19–24. doi:10.1109/maes.2004.1269687.

[67] J.-Q. Huang, T.-Z. Zhuang, Q. Zhang, H.-J. Peng, C.-M. Chen, F. Wei, Permselective graphene oxide membrane for highly stable and anti-self-discharge lithium–sulfur batteries, ACS Nano 9 (3) (2015) 3002–3011. doi:10.1021/nn507178a.

[68] M. L. Gordin, F. Dai, S. Chen, T. Xu, J. Song, D. Tang, N. Azimi, Z. Zhang, D. Wang, Bis(2,2,2-trifluoroethyl) ether as an electrolyte co-solvent for mitigating self-discharge in lithium–sulfur batteries, ACS Applied Materials & Interfaces 6 (11) (2014) 8006–8010. doi:10.1021/am501665s.

[69] C. Maurer, W. Commerell, A. Hintennach, A. Jossen, Continuous shuttle current measurement method for lithium sulfur cells, Journal of The Electrochemical Society 167 (9) (2020) 090534. doi:10.1149/1945-7111/ab8e81.

[70] D. D. Macdonald, Reflections on the history of electrochemical impedance spectroscopy, Electrochimica Acta 51 (8-9) (2006) 1376–1388. doi:10.1016/j.electacta.2005.02.107.

[71] Y. F. Pulido, C. Blanco, D. Anseán, V. M. García, F. Ferrero, M. Valledor, Determination of suitable parameters for battery analysis by electrochemical impedance spectroscopy, Measurement 106 (2017) 1–11. doi:10.1016/j.measurement.2017.04.022.

[72] A. Lasia, Electrochemical Impedance Spectroscopy and its Applications, Springer US, Boston, MA, 2002, pp. 143–248. doi:10.1007/0-306-46916-2_2.
URL https://doi.org/10.1007/0-306-46916-2_2

[73] V. Kolosnitsyn, E. Kuzmina, E. Karaseva, S. Mochalov, A study of the electrochemical processes in lithium–sulphur cells by impedance spectroscopy, Journal of Power Sources 196 (3) (2011) 1478–1482. doi:10.1016/j.jpowsour.2010.08.105.

[74] L. Yuan, X. Qiu, L. Chen, W. Zhu, New insight into the discharge process of sulfur cathode by electrochemical impedance spectroscopy, Journal of Power Sources 189 (1) (2009) 127–132. doi:10.1016/j.jpowsour.2008.10.033.

[75] Z. Deng, Z. Zhang, Y. Lai, J. Liu, J. Li, Y. Liu, Electrochemical impedance spectroscopy study of a lithium/sulfur battery: Modeling and analysis of capacity fading, Journal of The Electrochemical Society 160 (4) (2013) A553–A558. doi:10.1149/2.026304jes.

[76] K. Mc Carthy, H. Gullapalli, T. Kennedy, Online state of health estimation of li-ion polymer batteries using real time impedance measurements, Applied Energy 307 (2022) 118210. doi:https://doi.org/10.1016/j.apenergy.2021.118210.
URL https://www.sciencedirect.com/science/article/pii/S030626192101477X

[77] S. Kim, Y. Y. Choi, J.-I. Choi, Impedance-based capacity estimation for lithium-ion batteries using generative adversarial network, Applied Energy 308 (2022) 118317. doi:https://doi.org/10.1016/j.apenergy.2021.118317.
URL https://www.sciencedirect.com/science/article/pii/S0306261921015725

[78] D. Andre, M. Meiler, K. Steiner, H. Walz, T. Soczka-Guth, D. Sauer, Characterization of high-power lithium-ion batteries by electrochemical impedance spectroscopy. II: Modelling, Journal of Power Sources 196 (12) (2011) 5349–5356. doi:10.1016/j.jpowsour.2010.07.071.

[79] V. Knap, D.-I. Stroe, R. Purkayastha, S. Walus, D. J. Auger, A. Fotouhi, K. Propp, Reference performance test methodology for degradation assessment of lithium-sulfur batteries, Journal of The Electrochemical Society 165 (9) (2018) A1601–A1609. doi:10.1149/2.0121809jes.

[80] V. Knap, T. Kalogiannis, R. Purkayastha, S. Bęczkowski, D. I. Stroe, E. Schaltz, R. Teodorescu, Transferring the incremental capacity analysis to lithium-sulfur batteries, ECS Transactions 77 (11) (2017) 1919–1927. doi:10.1149/07711.1919ecst.

[81] J.-L. Dellis, Zfit, MATLAB Central File Exchange (2021).
URL https://www.mathworks.com/matlabcentral/fileexchange/19460-zfit

[82] D. Capkova, V. Knap, A. S. Fedorkova, D.-I. Stroe, Analysis of 3.4 ah lithium-sulfur pouch cells by electrochemical impedance spectroscopy, Journal of Energy Chemistry 72 (2022) 318–325. doi:10.1016/j.jechem.2022.05.026.

[83] S. Waluś, C. Barchasz, J.-F. Colin, J.-F. Martin, E. Elkaïm, J.-C. Leprêtre, F. Alloin, New insight into the working mechanism of lithium–sulfur batteries: in situ and operando x-ray diffraction characterization, Chemical Communications 49 (72) (2013) 7899. doi:10.1039/c3cc43766c.

[84] X.-B. Cheng, J.-Q. Huang, H.-J. Peng, J.-Q. Nie, X.-Y. Liu, Q. Zhang, F. Wei, Polysulfide shuttle control: Towards a lithium-sulfur battery with superior capacity performance up to 1000 cycles by matching the sulfur/electrolyte loading, Journal of Power Sources 253 (2014) 263–268. doi:10.1016/j.jpowsour.2013.12.031.

[85] T. O'Haver, peakfit.m, MATLAB Central File Exchange (2022).
URL https://www.mathworks.com/matlabcentral/fileexchange/23611-peakfit-m

[86] V. Knap, T. Zhang, D. I. Stroe, E. Schaltz, R. Teodorescu, K. Propp, Significance of the capacity recovery effect in pouch lithium-sulfur battery cells, ECS Transactions 74 (1) (2016) 95–100. doi:10.1149/07401.0095ecst.

[87] M. Marinescu, L. O'Neill, T. Zhang, S. Walus, T. E. Wilson, G. J. Offer, Irreversible vs reversible capacity fade of lithium-sulfur batteries during cycling: The effects of precipitation and shuttle, Journal of The Electrochemical Society 165 (1) (2017) A6107–A6118. doi:10.1149/2.0171801jes.

[88] S.-H. Chung, A. Manthiram, Bifunctional separator with a light-weight carbon-coating for dynamically and statically stable lithium-sulfur batteries, Advanced Functional Materials 24 (33) (2014) 5299–5306. doi:10.1002/adfm.201400845.

[89] C. Shen, J. Xie, M. Zhang, P. Andrei, M. Hendrickson, E. J. Plichta, J. P. Zheng, Self-discharge behavior of lithium-sulfur batteries at different electrolyte/sulfur ratios, Journal of The Electrochemical Society 166 (3) (2019) A5287–A5294. doi:10.1149/2.0461903jes.

[90] K. Propp, D. J. Auger, A. Fotouhi, M. Marinescu, V. Knap, S. Longo, Improved state of charge estimation for lithium-sulfur batteries, Journal of Energy Storage 26 (2019) 100943. doi:10.1016/j.est.2019.100943.

[91] S. S. Zhang, Role of LiNO3 in rechargeable lithium/sulfur battery, Electrochimica Acta 70 (2012) 344–348. doi:10.1016/j.electacta.2012.03.081.

[92] A. Fotouhi, D. J. Auger, K. Propp, S. Longo, Lithium–sulfur battery state-of-charge observability analysis and estimation, IEEE Transactions on Power Electronics 33 (7) (2018) 5847–5859. doi:10.1109/tpel.2017.2740223.

[93] W. Wang, Y. Wang, Y. Huang, C. Huang, Z. Yu, H. Zhang, A. Wang, K. Yuan, The electrochemical performance of lithium–sulfur batteries with LiClO4 DOL/DME electrolyte, Journal of Applied Electrochemistry 40 (2) (2009) 321–325. doi:10.1007/s10800-009-9978-z.

[94] N. A. Cañas, K. Hirose, B. Pascucci, N. Wagner, K. A. Friedrich, R. Hiesgen, Investigations of lithium–sulfur batteries using electrochemical impedance spectroscopy, Electrochimica Acta 97 (2013) 42–51. doi:10.1016/j.electacta.2013.02.101.

[95] C. Barchasz, J.-C. Leprêtre, F. Alloin, S. Patoux, New insights into the limiting parameters of the li/s rechargeable cell, Journal of Power Sources 199 (2012) 322–330. doi:10.1016/j.jpowsour.2011.07.021.

[96] X. Qiu, Q. Hua, L. Zheng, Z. Dai, Study of the discharge/charge process of lithium–sulfur batteries by electrochemical impedance spectroscopy, RSC Advances 10 (9) (2020) 5283–5293. doi:10.1039/c9ra10527a.